actuators

MDPI

Article

Development and Testing of a Linear Actuator for Acoustical Analysis of Hard Cheeses

Andrea Toscani *, Nicola Delmonte, Carlo Concari, Giorgia Mercati and Giovanni Chiorboli

Department of Engineering and Architecture, University of Parma, 43124 Parma, Italy; nicola.delmonte@unipr.it (N.D.); carlo.concari@unipr.it (C.C.); giorgia.mercati@studenti.unipr.it (G.M.); giovanni.chiorboli@unipr.it (G.C.)

* Correspondence: andrea.toscani@unipr.it; Tel.: +39-0521-906007

Abstract

Electromagnetic linear actuators are widely used in applications requiring fast, repeatable, and controlled mechanical excitation. This work proposes and experimentally validates a current-controlled actuation methodology for generating controlled and repeatable mechanical excitation for the automated acoustical inspection of hard cheeses. The proposed system is based on a push-type solenoid actuator driven by a closed-loop converter that generates a predefined current profile to obtain a controlled impact force on wheel cheeses. The system development was approached based on actuator simulations using the finite element method (FEM). This allows us to analyze the electromagnetic force generation process to identify the current waveform that produces an effective impact while ensuring vibration-free plunger return and avoiding bouncing at the end of its stroke. For acoustic measurements, a synchronized four-microphone acquisition system based on A2B was integrated. A preliminary experimental campaign to validate the concept and the development approach was conducted on a wheel of aged Pecorino cheese. The acquired acoustic responses showed highly repeatable impacts, with intra-class spectral variations below 1 dB under identical experimental conditions. Furthermore, the increase in damage artificially introduced on the tested cheese wheel caused measurable shifts in resonance frequencies, variations in spectral amplitudes, and the appearance of defect-related resonances. The results demonstrate the feasibility of the proposed approach for objective, repeatable, and non-destructive acoustic inspection of hard cheeses, providing a basis for future automated quality assessment systems.

Keywords: linear electromagnetic actuator; solenoid actuator; closed-loop current control; actuator force control; force profile optimization; A2B bus; acoustic excitation; acoustic monitoring; non-destructive testing

Check for updates

Academic Editors: Guichao Yang and Zhenle Dong

Received: 29 June 2026
Revised: 15 July 2026
Accepted: 24 July 2026
Published: 27 July 2026

Copyright: © 2026 by the authors. Licensee MDPI, Basel, Switzerland. This article is an open access article distributed under the terms and conditions of the Creative Commons Attribution (CC BY) license.

1. Introduction

The dairy sector represents a significant portion of the global agri-food economy, with a Compound Annual Growth Rate (CAGR) of approximately 5.8% [1,2]. In some countries, such as Italy, dairy production has been growing steadily in recent years and remains a key pillar of the national economy [3].

Overall, numerous varieties of cheese differ in their production, maturation, and texture. Among these are hard cheeses such as Parmigiano Reggiano, Grana Padano, and Pecorino Romano. These cheeses occupy a key role in global trade due to their value. These cheeses are characterized by a complex production process, which includes a long

maturation period, resulting in a compact internal structure. This structure makes it difficult to identify any internal defects. Historically, one of the most effective non-invasive methods has been pounding, introduced to inspect and select Parmigiano Reggiano [4]. This procedure involves an expert listening to the sound the cheese wheels make, as if they were drums, when struck with a special hammer. The experience of the pounder is essential to distinguishing flawless cheeses from those with imperfections. This selection process is effective because it can be carried out quickly, but it does have some drawbacks. The most significant is that the sound varies with maturation, and only an expert's ear can quickly detect this variability. Considering that just under 10 million wheels of Grana Padano and Parmigiano Reggiano are produced each year (see data in Table 1), the speed of the inspection and selection process is extremely important. The number of wheels produced annually increases over the years, but the number of experienced workers, called "beaters", from the consortia that issue the labels to be printed on cheese wheels does not increase proportionally. Thus, active beaters have to examine a large number of wheels in a short time, increasing the risk of analysis errors. This often leads to the rejection of wheels suitable for sale at full price, thus generating significant economic losses for producers. Therefore, the introduction of automatic inspection and selection systems is becoming increasingly important.

Table 1. Parmigiano Reggiano and Grana Padano production data in 2024 (Source: [5]).

Figures of Merit	Parmigiano Reggiano	Grana Padano
Processed milk [Mt]	2.04	2.95
Number of farmers supplying milk	2103	3576
Number of producing dairies	291	135
Number of cheese wheels produced	4,079,248	5,635,153
Change compared to 2023	+1.62%	+3.27%
Gross Saleable Production [€ billion]	3.2	4.0

As shown in Section 2 of this article, various techniques have been developed in recent years for the inspection and selection of cheeses. Unlike all of these, the one presented in this article is based on the technique used by cheese beaters. It has several advantages over the others presented in the following section: (i) it is non-invasive (the microbial activity that allows maturation and development in cheese is not affected) and is non-destructive; (ii) it is easily replicable and repetitive; (iii) its energy consumption is quite low.

The remainder of the paper is structured as follows. The next section is dedicated to a brief review of the state-of-the-art cheese characterization methods and solenoidal linear actuators for controlled impact generation. The scientific contribution of this work lies in the definition and validation of an integrated methodology for automated acoustical inspection based on optimized electromagnetic excitation. Rather than focusing solely on hardware implementation, the proposed approach combines physics-based actuator optimization, closed-loop force control, and quantitative acoustic validation to obtain a repeatable excitation suitable for non-destructive inspection. The definition and validation of an integrated methodology for automated acoustic analysis based on optimized electromagnetic excitation for the sorting of hard cheeses is the scientific contribution of this work. Rather than focusing solely on hardware implementation, the proposed approach combines physics-based actuator optimization, closed-loop force control to achieve repeatable excitation, and quantitative acoustic validation in the frequency domain.

Section 3 describes the materials and methods used and applied in this work to develop the proposed system for hard cheese classification. More specifically, this section presents, in addition to the chosen push solenoid, the numerical models used for the system design

and the results obtained from their simulations. Section 4 shows the results obtained from a preliminary test performed on a wheel of aged Pecorino cheese. Lastly, the conclusions chapter summarizes the system development methodology and the results achieved.

2. State-of-the-Art

2.1. Cheese Characterization Techniques

Cheese analysis can be useful during production to monitor ripening and for accurate selection, discerning the quality of these products. For this reason, several studies on this topic can be found in the literature, demonstrating the results obtained with various proposed and tested investigation techniques. Given the proliferation of techniques and solutions, some have even written reviews on the topic. Among these, the most interesting are those by J. Ahranjani et al. [6], who focused on spectroscopic techniques for detecting adulteration, and by T. Lei and D.W. Sun [7], who instead analyze non-destructive techniques for evaluating quality attributes.

A variety of techniques are available. Wet chemistry and other infrared spectroscopy-based analysis methods, such as optothermal near-infrared (NIR) and Fourier transform mid-infrared-attenuated total reflection (FTIR-ATR), were already being used in the 1980s and 1990s. These methods were tested in [8]. This study compares two rapid infrared techniques for measuring the amounts of fat, protein, and water present in 24 different cheeses, from soft to hard. Optothermal NIR performed better (correlation coefficient = 0.93–0.96 and standard error prediction = 2–5%) than FTIR-ATR (correlation coefficient = 0.81–0.92 and standard error prediction = 4–9%), mainly due to the heterogeneity of the cheese, especially due to the micrometric fat globules. At the time, they discovered that with FTIR-ATR, the penetration depth was comparable to the size of the fat globules. Therefore, small microstructural variations significantly altered the signal. In optothermal NIR, the investigated volume is larger, and the effect of heterogeneity is reduced. The optothermal NIR method was deemed more robust, faster, cheaper, and suitable for direct industrial use.

Improved technologies have also led to improvements in FTIR-ATR tools. So much so that in 2010, M.J. Lerma-García et al. [9] presented a study in which FTIR-ATR spectroscopy combined with linear discriminant analysis (LDA) of the spectral data was applied to Italian Pecorino cheeses for their classification according to ripening times. As shown, the classification was excellent, with an accuracy greater than 95% and a clear separation of the identified Pecorino categories. Thus, this study demonstrated that the FTIR-based method can be used for authentication, quality control, and ripening verification.

Around the same time, Cevoli et al. [10], again for the classification of Pecorino cheeses, presented a different method based on an electronic nose (e-nose) consisting of MOS sensors combined with an Artificial Neural Network (ANN).

The study aimed to develop a method for classifying Pecorino cheeses by maturation, production method, and ripening site ("fossa/non-fossa"). The proposed method, in addition to the e-nose and the ANN, involves the application of principal component analysis (PCA) and achieves correct classification with an RMSE of approximately 0.024. The results of the method were compared with those obtained with gas chromatography–mass spectrometry (GC–MS), also with ANN, which showed a lower accuracy than the e-nose (≈86%).

Centering the analysis of the state of the art on hard cheeses, the focus of this study, three other works in the literature are of interest. The first uses thermogravimetry (TG) and derived thermogravimetry (DTG) to determine the water present in the cheese matrix, low-resolution nuclear magnetic resonance (NMR), and high-resolution NMR to determine the location of the water to assess the amino acids present in the cheese wheel, respectively [11].

The proposed system allows for the identification of free and bound water, which is important because water activity is linked to microbial growth and enzyme action and affects the ripening process. NMR allows for the distinction between intra-micellar and inter-micellar aqueous fractions, as well as the saturated/unsaturated lipid fractions that change with ripening. Furthermore, high-resolution NMR allows for the simultaneous quantification of free amino acids, whose variations reflect proteolysis and enzymatic activity, which differ significantly between the center and periphery of the cheese wheel.

V. Maestrello et al. [12] investigated the use of an untargeted NMR-based metabolomics approach to detect the compositional changes of Grana Padano during ripening and to quantitatively evaluate the impact of bactofugation on the cheese's metabolic profile. Thus, NMR metabolomics is proposed as a quantitative, objective, and multidimensional tool for the control of PDO cheeses.

More recently, Chuquizuta et al. [13] compared the results obtained with dielectric spectroscopy and those obtained with NIR to predict the ripening time of Swiss-type cheese. In this work, dielectric spectroscopy outperforms NIR in almost all parameters: prediction of ripening days, color prediction, and texture, which is the most difficult to model. From a physical point of view, this can be explained because ripening modifies free water, proteins, lipids, as well as electrical polarization and ion mobility, and dielectric spectroscopy is very sensitive to these profound structural transformations [13]. The study proposes dielectric spectroscopy as an emerging technology for inline monitoring with automated real-time control of ripening.

Based on the articles analyzed in the literature review, "non-destructive" often means that the proposed technique itself does not chemically degrade the material. This, however, does not necessarily imply the absence of sampling or cutting of the cheese, and that the sample is still edible at the end of the analysis.

For the dairy sector, the practical value scale is shown in Table 2.

Table 2. Level of invasiveness of techniques to characterize cheeses during ripening.

Level of Invasiveness	Characterization Technique
Non-invasive	Inline External Imaging, X-rays
Minimally Invasive	NIR, e-nose, low-res NMR
Semi-destructive	FTIR-ATR, dielectric
Destructive	Metabolomic NMR, TG, wet chemistry

Furthermore, the studies reviewed allow us to make several considerations. First of all, the most effective emerging techniques are infrared, hyperspectral imaging (computer vision, tomography, X-ray, magnetic resonance), electronic noses, and dielectric spectroscopy. Instead, the most monitored variables are the cheese's components (fat, water, proteins, amino acids, and aromatic compounds), rather than its texture, color, and degree of ripeness.

In recent years, mathematical models and more standard analyses such as principal component analysis (PCA), partial least squares regression (PLSR), and linear discriminant analysis (LDA) have been increasingly joined by artificial intelligence techniques such as ANNs and machine learning [6,7]. The evolution of the sector is moving towards portable sensors, rather than inline systems, to perform non-destructive analyses. Demand from large producers is increasingly moving toward the development of automated quality control systems with the digitalization of the entire production chain [14]. This shift can be referred to as "Dairy 4.0," aligning with the broader context of the fourth industrial revolution.

To monitor aging, the nearly thousand-year-old technique of "listening" to the sound produced by a hard cheese like Parmigiano Reggiano has not yet been applied with automatic machines. The work presented here, which involves controlled activation of a push solenoid as if it were a drumstick to beat the wheel, goes precisely in this direction.This method for monitoring the ripening of hard cheeses has several advantages:

- The system is very simple (drive circuitry, a push solenoid hammer, microphones, a sound acquisition system with frequency processing, and a mechanical structure to support the microphones and hammer);
- It is neither destructive nor invasive;
- It requires little energy;
- It can provide results within a few seconds;
- It is not harmful to humans;
- It complies with the production specifications of some dairy consortia, which aim to preserve production and products as they were originally produced, without the use of industrial machinery.

While the previously reviewed studies mainly focus on analytical and sensing techniques for cheese characterization and quality assessment, the effectiveness of the proposed automated beating system also strongly depends on the capability of the excitation mechanism to generate controlled, repeatable, and reliable impacts. For this reason, it is essential to examine the current state of the art of linear electromagnetic actuators and the control strategies adopted to optimize their dynamic performance.

2.2. Solenoidal Linear Actuators for Controlled Impact Generation

Electromagnetic linear actuators and solenoids are widely employed in industrial applications requiring fast, repeatable, and compact linear motion. Their dynamic performance is strongly influenced by the nonlinear relationship between excitation current, armature position, and generated electromagnetic force, making accurate modeling and control essential for high-performance operation.

Current-controlled actuation has become increasingly attractive because it enables direct regulation of the generated electromagnetic force while compensating for variations caused by armature displacement and magnetic nonlinearities [15].

Recent studies have focused on the development of analytical and finite-element models capable of predicting the force characteristics of push–pull solenoids and supporting actuator design optimization [16,17]. Furthermore, several authors have demonstrated that actuator performance can be significantly improved through optimized current excitation strategies and electromagnetic design techniques aimed at increasing force generation and reducing response time [18,19].

In applications involving controlled impacts or rapid mechanical excitation, the rise time of the electromagnetic force becomes a critical parameter. Previous research has shown that current waveform shaping and force optimization techniques can substantially improve the transient response of solenoid actuators, enabling faster and more repeatable actuation cycles [18,20,21]. In particular, finite-element-based optimization approaches have been successfully employed to maximize thrust force while maintaining compact actuator dimensions and low power consumption [16,19,22,23].

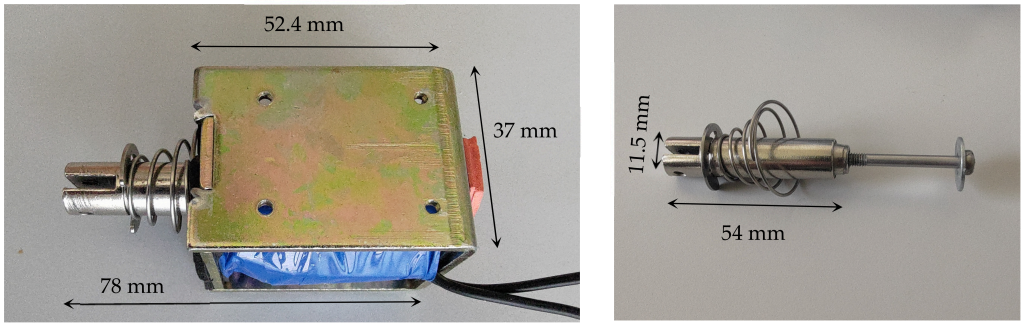
The generation of repeatable impacts is particularly important in non-destructive testing applications, where the consistency of the excitation directly affects measurement reliability. Despite the extensive literature on electromagnetic actuators and solenoid force control, the application of a current-controlled linear electromagnetic actuator for automated cheese tapping and acoustical inspection of hard cheeses has received very limited attention. Therefore, this work proposes a dedicated actuation system based on a

push–pull solenoid driven by a closed-loop current-controlled power converter capable of generating a precisely shaped force profile, reproducing the tapping action traditionally performed by expert cheese inspectors.

3. Materials and Methods

The proposed methodology consists of four sequential stages: (i) FEM-based optimization of the actuator excitation profile, (ii) implementation of a closed-loop current-controlled drive, (iii) synchronized multi-microphone acoustic acquisition, and (iv) experimental validation through repeatability analysis and controlled defect detection.

The task of delivering the strike to the cheese wheel is performed by a linear actuator, specifically an open-frame push solenoid (Heschen HS-1250). According to the manufacturer's specifications, the actuator is rated for 12 V DC operation, a nominal current of 3 A, and a 10 mm stroke (Figure 1).



(**a**) (**b**)

Figure 1. Linear actuator, Heschen HS-1250 push-type solenoid. (**a**) whole open-frame solenoid; (**b**) internal plunger.

Because the strike must be precisely controlled and executed within a very short time interval, and because the shaft is required to return slowly and smoothly to its resting position in order to prevent unwanted noise and mechanical vibrations generated by the return spring, precise control of the supply current is essential. This allows not only proper timing and force of the actuation, but also improved reliability, reduced mechanical stress, and overall quieter operation of the system.

To determine the optimal current profile required to achieve an effective and well-controlled strike, a series of FEM simulations were conducted. These simulations made it possible to accurately characterize and quantify the relationship between the force generated by the shaft and the current supplied to the solenoid, providing valuable insights for optimizing performance, improving control accuracy, and ensuring consistent and reliable operation of the system.

3.1. Finite Element Model

The finite element model (FEM) was implemented using the Magnetic Fields interface of COMSOL Multiphysics v. 5.3. This was used to compute the magnetic field and induced current distributions within the push–pull solenoid domain. The latter was simplified by assuming that the external frame is cylindrical, as are the coil and plunger shaft. This allows the structure to be analyzed in a two-dimensional domain (see Figure 2) by exploiting the assumption of cylindrical symmetry.

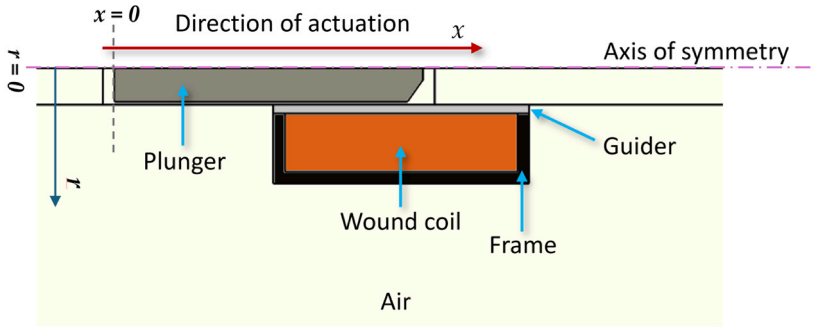


Figure 2. Pull solenoid 2D geometry drawn in COMSOL Multiphysics.

The plunger was modeled as being made of low-carbon steel 1002 with the BH curve fully saturated at 2 T. The screw at the head of the plunger was neglected due to its diameter of 2.5 mm. Further details of the materials set in the FEM model are reported in Table 3.

Table 3. Magnetic parameters set in the FEM model.

Part	Material	Relative Permeability	Magnetic Field and Co-Energy Density
Plunger	Low-carbon steel 1002	4000	BH curve (B_{max} = 2 T)
Wound coil	Copper	1	-
Frame	Soft iron with losses	1200	BH curve (B_{max} = 2.4 T)
Guider	Non-ferromagnetic	1	-
External environment	Air	1	-

The FEM model calculates magnetic and induced current distributions by solving Maxwell's equations with the magnetic vector potential $\overline{A}$ as the dependent variable. The equation set solved for a time-dependent analysis is:

- Ampère's law

$$\nabla \times \overline{H} = \overline{J} \quad (1)$$

where $\overline{H}$ is the magnetic field, and $\overline{J}$ is the current density.

- Magnetic flux density

$$\overline{B} = \nabla \times \overline{A} \quad (2)$$

- Total current density

$$\overline{J} = \sigma \overline{E} + \sigma \overline{u} \times \overline{B} + \overline{J}_e \quad (3)$$

where σ is the electric conductivity, $\overline{E}$ is the electric field, $\overline{u}$ is the speed of electrons moving in the magnetic field, and $\overline{J}_e$ is the externally applied current density.

- Faraday's law

$$\overline{E} = -\frac{\partial \overline{A}}{\partial t} \quad (4)$$

Ampère's law is the main equation, solved in all domains except in the wound coil, where the Multi-Turn Coil domain feature available in COMSOL Multiphysics is applied. The model of the Multi-Turn Coil represents a bundle of N turns (2400 in this case) of the wire used for the winding as a continuous macroscopic domain (homogenized multiturn). This approach eliminates the need to calculate the currents of each loop, which can be drawn in the winding domain, resulting in a geometry that requires discretization with a very large number of elements.

The Multi-Turn Coil can couple an external electrical constraint (current, voltage, or power) to the externally applied current density vector $\bar{J}_e$:

$$\bar{J}_e = \frac{NI_{coil}}{A}\bar{e}_{coil} \tag{5}$$

where N is the total number of coil turns, I_{coil} is the total current passing through the coil wire, A is the total cross-sectional area of the coil window, and $\bar{e}_{coil}$ is a unit vector field representing the local direction of the wire winding at each point inside the domain.

In this case, we chose to apply I_{coil}. The primary objective of the FEM simulations was to identify the current pulse that must be generated by the drive to better generate the cheese pounding strokes. The pulse used in the pounding tests will be shown later.

The magnetic force applied to the plunger was determined by applying the appropriate COMSOL Multiphysics feature that calculates it through the Maxwell Stress Tensor [24].

To simulate the plunger's motion dynamics, we used the Global ODEs and DAEs interface, enabling us to solve time-dependent ordinary differential equations (ODEs) and differential-algebraic equations (DAEs) without space dependency. Indeed, the plunger's motion can be determined by modeling the push solenoid as a mass-spring-damper system plus the magnetic force (F_{mag}) produced by the current flowing in the wound coil. Therefore, the plunger's instantaneous position (see Figure 2) and velocity can be obtained by solving the following equations:

$$m\frac{dv}{dt} + cv + kx - F_{mag} = 0 \tag{6}$$

$$\frac{dx}{dt} - v = 0 \tag{7}$$

where m is the plunger's mass, v is its velocity, x is the instantaneous position, k is the spring constant (set to 800 N/m), and c is the viscous damping coefficient (set to the critical value $2\sqrt{mk}$).

To simulate the plunger's motion, the mesh was set as shown in Figure 3. The prescribed deformation was set to be equal to the instantaneous position along the x direction.

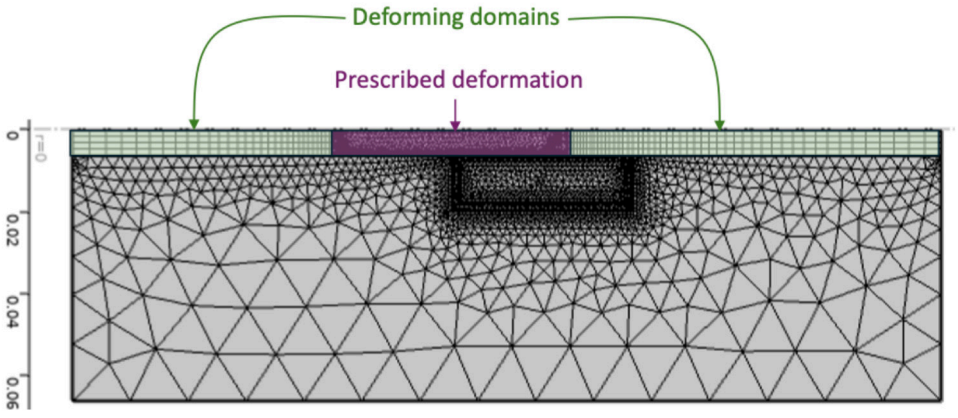


Figure 3. Mesh of the pull solenoid 2D geometry used for simulations. It is composed of 9450 elements (1522 rectangles and 7928 triangles).

Assuming that the cheese is placed 10 mm from the tip of the plunger, the objective of the FEM analysis was to verify which current ramp is adequate to impact the cheese with a kinetic energy similar to one generated by the human beaters with their hammer, and, after a time of a few tens of milliseconds deemed necessary for a good transfer of energy to the cheese so that it vibrates, identify the current descent to return the plunger to its resting

position without triggering the limit switch. This would avoid any rebounds that could produce undesirable noise. To achieve this, several parametric simulations were carried out varying: (i) maximum current value; (ii) the rise time of the current pulse; (iii) the fall time of the same pulse.

The current profile identified through the FEM simulations is illustrated in Figure 4. The rising edge of the current is designed to be as fast as possible in order to generate a sharp and well-defined impact, ensuring the effectiveness of the strike. In contrast, the falling edge is intentionally made slower and carefully controlled, allowing the system to return smoothly to its resting condition while minimizing noise, reducing mechanical stress, and preserving the operational benefits discussed previously.

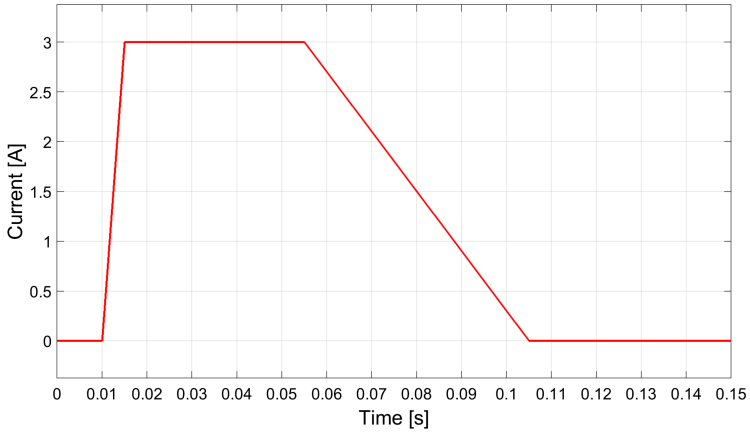


Figure 4. Optimized current profile for driving the linear actuator.

Figure 5 shows the results from the simulation, with the current pulse chosen to optimize plunger driving. As can be observed, a large portion of the plunger enters magnetic saturation during the current rise, approximately 4 ms after the start of the ramp, when the current is 2.4 A. Figure 6 shows the limit situation for magnetization with the current equal to 3 A. Here, it can be observed that the part with a magnetic flux density greater than 1.5 T, a value beyond which BH curve of the low-carbon steel 1002 is no longer linear and has lower slope, occupies almost the entire cross-section of the plunger.

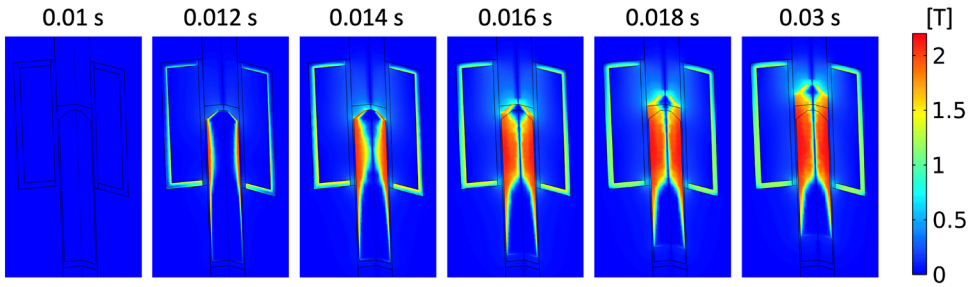


Figure 5. Magnetic flux density distributions obtained from FEM simulations at different time instants during the application of the optimized current pulse of Figure 4. At 30 ms, we observed the maximum displacement of the plunger.

The most important insights that can be obtained from the FEM simulation for the actuator to be implemented are those of the quantities represented in Figure 7. From the time graphs displayed here, some observations can be made.

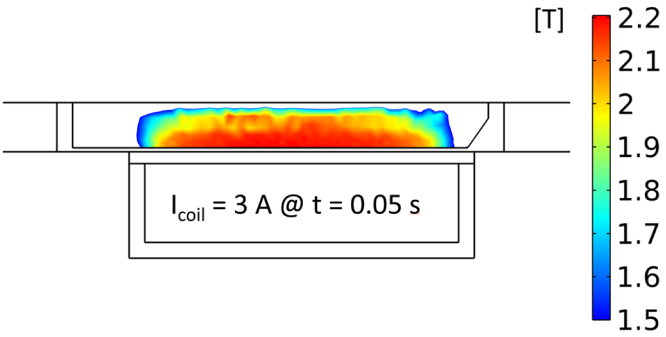


Figure 6. Simulated magnetic flux density in the plunger greater than 1.5 T at t = 0.05 s when the current in the coil is equal to 3 A.

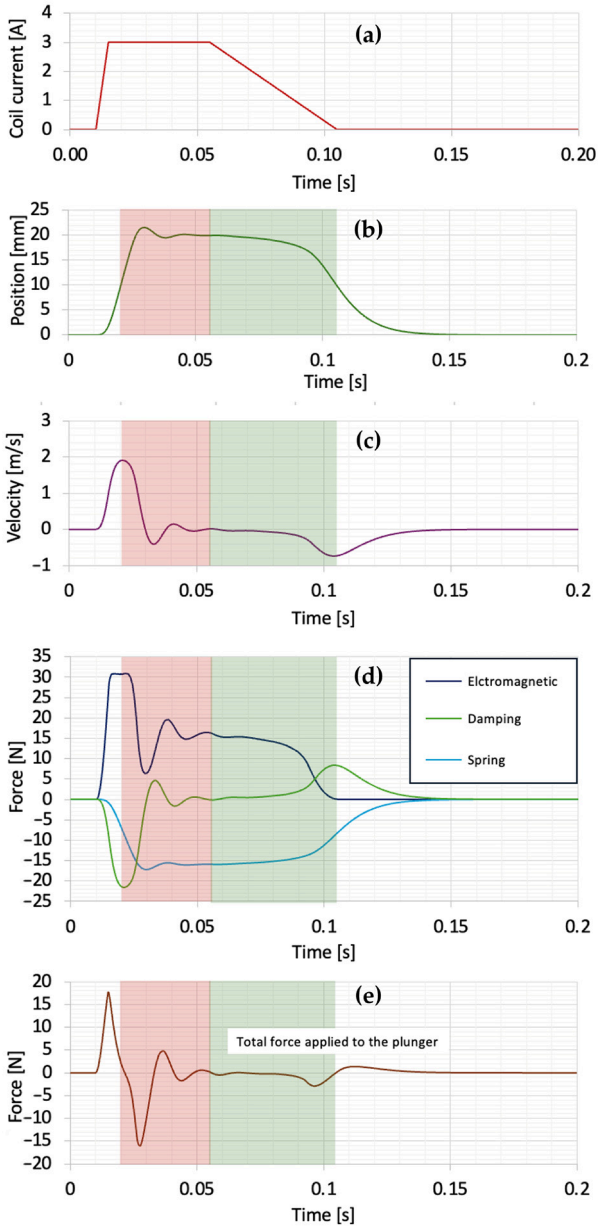


Figure 7. FEM simulation results applying the coil current (**a**) to the solenoid: (**b**) position; (**c**) velocity; (**d**) electromagnetic, damping, and spring forces; (**e**) total force applied to the plunger.

Firstly, during the time interval identified by the pink band, which occurs between the moments when the position exceeds 10 mm and the current is kept at 3 A, it is not

related to what will happen in the real case because the cheese will not allow the plunger to move more than 10 mm. Within the green band, in the real case with the stop at 10 mm, a different dynamic trend is expected, returning to a similar one when it ends.

The contact interaction between the plunger and the cheese was intentionally not included in the FEM model. The objective of the numerical analysis was to optimize the actuator dynamics up to the instant of impact and to determine the current waveform required for repeatable excitation. Since the actuator is driven by a closed-loop current-controlled converter, the prescribed current profile is actively regulated despite the mechanical interaction occurring at impact. Consequently, the cheese stiffness mainly influences the post-impact mechanical response and the transfer of energy to the specimen, whereas the repeatability of the excitation is ensured by the current-controlled actuation and was ultimately verified experimentally.

Additionally, the slope of the current rise ramp allows the maximum current value to be reached almost simultaneously with the time necessary to have the maximum speed, then the maximum kinetic energy right at the actual end stop of 10 mm.

Finally, the plunger goes back more gradually, decelerating smoothly until it reaches its rest position without bouncing.

3.2. Behavioral Model of the Actuator

The conventional method for driving the linear actuator consists of using a voltage generator applying a voltage equal to its nominal value of 12 V. Under these conditions, the steady-state current can reach its nominal value of approximately 3 A. However, the current does not change instantaneously because, even when applying a voltage step, it follows the typical exponential behavior of an RL transient, meaning that the current rises and settles according to the inductive characteristics of the system, rather than responding immediately to the applied voltage.

Using this driving approach, the current and then the force generated by the actuator increase gradually. As a result, the impact may be less crisp than necessary to achieve the precise, well-defined "snap" that would be desirable for a beat that effectively vibrates the cheese wheel.

For this reason, a higher driving voltage (24 V) was adopted in combination with a closed-loop current control strategy capable of accurately shaping the desired current profile. This approach makes it possible to directly regulate the force generated during the impact, ensuring a more precise and effective strike. At the same time, it allows the system to overcome the inherent RL dynamics of the actuator, which would otherwise limit the speed of current variation and reduce the responsiveness of the actuation.

The architecture of the proposed power converter is shown in Figure 8; it is a step-down (buck) converter topology. On the left side, the input voltage source (V_{in1}) provides the supply, which is filtered by an input capacitor (C_{in}) along with its equivalent series resistance (C_{inESR}) and a series resistance representing the source impedance ($R_{inVsource}$). The central element of the circuit is a switching device, whose gate is driven by a control signal (V_{gate}). This MOSFET operates as the main switching component, regulating the energy transferred from the input to the load. A diode (D_1) is connected in a freewheeling configuration to circulate the current of the inductive load when the MOSFET is turned off. On the output side, to simulate the electrical behavior of the linear actuator, the load is modeled as an inductor (L_{out}) in series with a resistor (R_{out}). The output voltage (V_{out}) and the output current (I_{out}) are monitored through a voltage measurement block and a current measurement block, respectively.

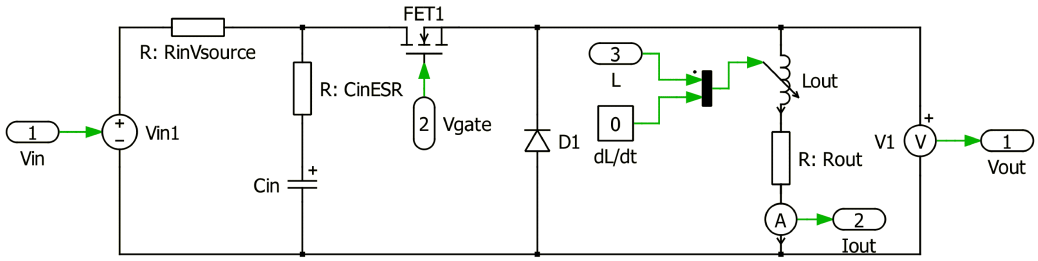


Figure 8. Proposed power converter for driving the linear actuator.

The inductor value L_{out} depends on the position $x(t)$ of the plunger: for a long solenoid with a uniform magnetic field and a constant cross-sectional area A, neglecting fringes and saturation, we would find that the reluctance varies linearly with the position of the plunger, and therefore the inductance can be assumed inversely proportional to $k_\mu - x$, where k_μ is a constant. For this reason, the magnetic force—which can be obtained as the derivative of the co-energy with respect to the position x and thus as $F_{mag} = 0.5\ I^2 dL/dx$—can be expressed as [25]:

$$F_{mag} = \frac{k_{sol}}{\left(k_\mu - x\right)^2} I^2 \tag{8}$$

However, saturation and fringing effects are present, and even though the current transient is not instantaneous, it is faster than the plunger's position transient, so we decided to interpolate the inductance linearly with the position.

The power converter is operated under a closed-loop current control scheme, implemented through a control architecture as depicted in Figure 9. This approach enables continuous monitoring and regulation of the output current, allowing the system to accurately track the desired current reference. As a result, it ensures precise control of the actuator force, improves dynamic response, and enhances the overall stability and performance of the system.

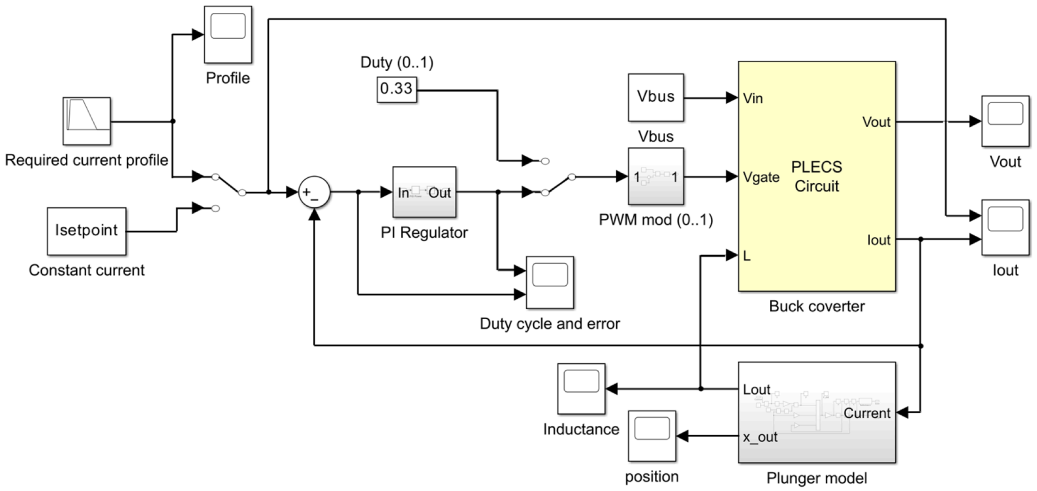


Figure 9. Block schematic of the current-controlled closed loop for driving the linear actuator.

The present work does not address the long-term aging of the actuator components, such as spring stiffness variations or mechanical wear. Nevertheless, the adoption of closed-loop current control reduces the influence of electrical parameter variations on the generated excitation by ensuring accurate tracking of the prescribed current waveform.

It should be noted that coil temperature monitoring and online resistance identification were not implemented in the present prototype. The experimental validation was

performed under laboratory conditions and did not include long-term continuous operation at thermal equilibrium. Nevertheless, since the actuator is driven by a closed-loop current-controlled converter, temperature-induced variations in coil resistance mainly affect the voltage duty cycle required to track the prescribed current waveform, while the generated electromagnetic force remains governed by the regulated current, provided that sufficient voltage margin is available and the actuator operates within its thermal limits. The integration of coil temperature monitoring and online resistance estimation will be considered in future developments to ensure force consistency under production-line operating conditions.

The system illustrated in Figure 9 was simulated using MATLAB/Simulink R2024b and PLECS Blockset v.4.1.3. These simulation tools were employed to accurately model both the control strategy and the power stage dynamics, enabling a detailed analysis of the system's behavior under various operating conditions and providing valuable insights for design validation and performance optimization.

3.3. Acoustic Acquisition System and Signal Preprocessing

The overall system setup scheme is illustrated in Figure 10a, the cheese wheel is positioned at the center of the test bed. In the present laboratory prototype, the solenoid actuator was mounted on a rigid support and manually aligned with the cheese wheel to maintain a fixed impact distance and orientation during the experimental campaign. For future industrial implementation, the actuator is intended to be integrated into a guided mechanical head with mechanical stops or compliant positioning elements, ensuring a constant stand-off distance, normal impact direction, and repeatable contact location on the cheese surface. This mechanical referencing strategy is necessary to preserve the excitation consistency provided by the current-controlled actuator under production-line conditions. The system is monitored by a four-microphone array specifically designed to evaluate the spatial directivity and the internal transmission of the acoustic response. All four microphones are uniformly positioned at a close distance of 7 cm from the cheese crust. This near-field configuration was deliberately selected for two main reasons: first, to maximize the signal-to-noise ratio (SNR) against environmental laboratory noise; second, to locally map the multidirectional propagation of the acoustic wave through the dense cheese matrix along distinct radial axes, rather than acquiring a blended global far-field resonance.

Although the proposed near-field configuration improves the signal-to-noise ratio by maximizing the acoustic energy captured from the impact event, the present experimental validation was conducted under laboratory conditions and does not reproduce the acoustic environment of an industrial production line. It should also be noted that the A2B-based acquisition system mainly contributes by providing synchronized, low-jitter, and electrically robust multichannel acquisition, whereas the mitigation of ambient acoustic noise relies primarily on the measurement geometry, time-windowed acquisition, and subsequent signal processing.

Geometrically, three microphones are spaced at approximately 90° intervals around the back and sides of the wheel. The fourth microphone completes this spatial setup at the front; due to the physical presence of the linear actuator, it is placed in close proximity to the contact point. This specific front sensor is tasked with capturing the localized initial impact excitation, seamlessly allowing for the subsequent temporal isolation of the impact sound from the actuator's mechanical return noise.

All microphone signals are collected using a Digital Acquisition Board (DAQ), which ensures synchronized and high-quality data acquisition. The recorded signals are then transferred to and stored on a laptop for subsequent processing and analysis, allowing both temporal and spectral characteristics of the impact sound to be thoroughly evaluated.

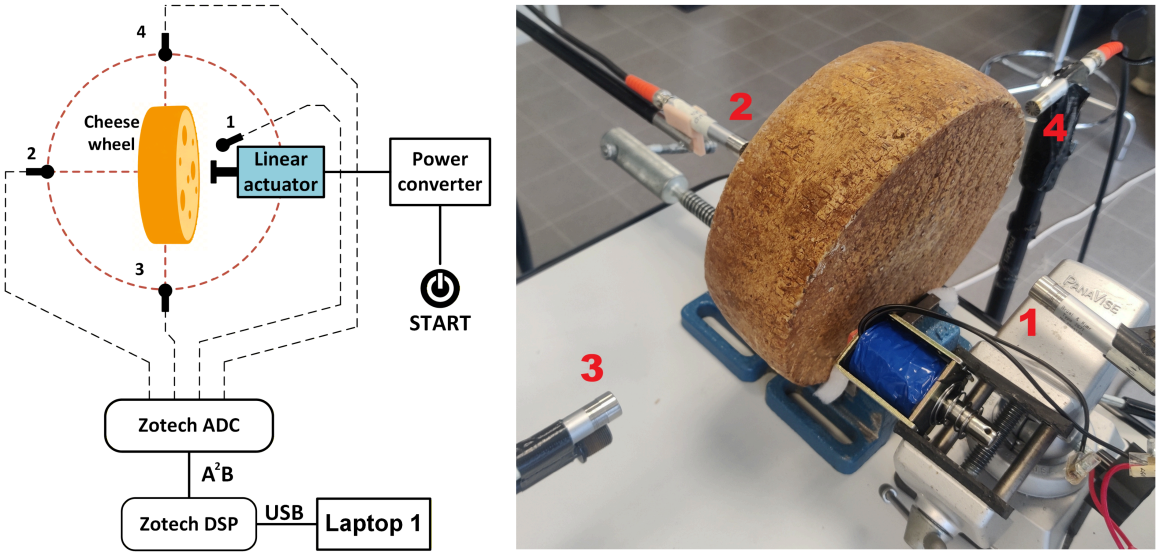


Figure 10. Overall system for the acoustical analysis: (**a**) block schematic including the linear actuator, the power converter, the microphones, and the digital acquisition system; (**b**) experimental test bed. The cheese wheel had a diameter of 22 cm and a heel height (thickness) of 8 cm.

The microphones are four Brüel & Kjær type 4188 omnidirectional microphones (Table 4); each of them was mounted on a rigid support to properly orient them and to eliminate unwanted parasitic vibrations.

Table 4. Microphone and Preamplifier Brüel & Kjær 4188-2176 technical data.

Specification	Value
Sensitivity	31.6 mV/Pa
Dynamic Range	19 to 138 dB
Frequency Range	8 Hz to 12.5 kHz

The four microphones forming the array need to be acquired at the same time, making strict synchronization across all channels essential. To fulfill this requirement, a DAQ system capable of maintaining precise timing alignment was necessary. Therefore, Zotech's DAQ system was selected, as it is based on Analog Devices' A2B bus [26], which supports the transmission of up to 32 channels sampled at 48 kHz with 24-bit resolution over a single Unshielded Twisted Pair (UTP) cable. Signal acquisition and routing were handled using Plogue Art et Technologie Bidule software (v0.9761), interfacing with the hardware via standard ASIO drivers. For all experimental tests, the A2B-based DAQ system was configured to simultaneously acquire the four microphone channels at a sampling rate of 48 kHz with a 24-bit resolution. This sample frequency provides a high temporal resolution (approximately 20.8 µs), which is essential to accurately capture the fast transients of the acquired acoustic Impulse Responses (IRs).

Although this DAQ platform was originally developed for automotive applications, it is highly versatile and can be effectively employed in several other domains. These include structural health monitoring [27], industrial condition monitoring [28,29], vibration analysis systems, and predictive maintenance applications, all of which typically require the simultaneous and real-time acquisition of a large number of sensors. In this context, the A2B-based DAQ system represents an efficient alternative for synchronous multi-channel acquisition, while also reducing overall system costs thanks to the use of inexpensive

cabling and dedicated low-cost transceivers. Due to these characteristics, A2B technology is particularly well suited for systems involving microphone arrays [30,31].

An additional advantage of the proposed architecture is the inherent synchronization capability of the Zotech ADC devices. The digital communication bus ensures that all nodes within the network remain tightly synchronized, with minimal latency and very low jitter levels [32]. Even in more complex setups [28,29], where there may be significant physical separation between the tachometer, accelerometer, and microphone array, the system is still able to guarantee accurate synchronization among all the acquired signals.

Following the acquisition, the raw acoustic signals were subjected to an offline preprocessing pipeline to isolate the pure structural response of the cheese from any environmental and mechanical artifacts. First, a time-domain windowing was applied to each acquired signal. Specifically, the Impulse Responses (IRs) were truncated to a precise length of 1600 samples. Considering the 48 kHz sampling rate, this corresponds to an observation window of approximately 33.3 ms. This strict temporal truncation was methodologically necessary to isolate the primary elasto-acoustic transient generated by the impact, entirely avoiding the contamination from the mechanical return noise of the actuator's plunger.

To eliminate DC offset and sub-audio environmental rumble, a high-pass filter with a cut-off frequency of 30 Hz was applied to the windowed signals. The time-domain sequences were subsequently transformed into the frequency domain using a Fast Fourier Transform (FFT). To ensure a high spectral interpolation and a smooth visualization of the resonant peaks, the 1600-sample arrays were zero-padded to an FFT length of N = 16,384 points. Furthermore, to reduce spectral variance and local noise, the magnitude spectra were processed using a moving average smoothing filter (rectangular window) spanning 15 consecutive frequency bins. The spectral analysis was bound to an upper frequency limit of 2 kHz. This boundary is physically justified by the dynamics of the mechanical excitation: the finite contact time between the actuator's plunger and the cheese crust acts inherently as a mechanical low-pass filter, preventing the efficient excitation of higher-order acoustic vibrational modes within the cheese matrix.

To mitigate the influence of narrow-band computational noise and isolate the macroscopic modal envelope of the cheese matrix, a rectangular moving average smoothing filter spanning $W = 15$ bins was applied directly to the individual magnitude spectra across the targeted 30–2000 Hz frequency band. Let $\widetilde{S}_k(f_j)$ denote the smoothed logarithmic spectrum of the k-th impact. The intra-class repeatability of the actuation system was then quantified using the Mean Absolute Error (MAE). For each structural condition, the ensemble average of the smoothed spectra, $\overline{\widetilde{S}}(f_j)$, was computed. The global scalar MAE was subsequently calculated as the arithmetic mean of the absolute deviations between each individual smoothed spectrum and the ensemble average:

$$MAE = \frac{1}{M \cdot N} \sum_{k=1}^{M} \sum_{j=1}^{N} \left| \widetilde{S}_k(f_j) - \overline{\widetilde{S}}(f_j) \right| \tag{9}$$

where $M = 4$ is the number of validated strikes and N represents the total number of frequency bins in the analyzed bandwidth. This approach ensures that the error metric quantifies the deterministic reliability of the mechatronic actuation purely based on the physical macroscopic divergence of the acoustic response, thereby reducing the influence of non-structural, high-frequency spectral fluctuations caused by residual measurement noise, slight impact-to-impact variability, and weakly excited frequency components, while preserving the dominant structural resonances of the cheese.

3.4. Experimental Protocol and Defect Simulation

Since the primary objective of this study is the validation of the automated actuation hardware, a proof-of-concept experimental protocol was designed to evaluate the system's sensitivity to macroscopic structural variations. The preliminary validation was conducted on a commercial aged Pecorino cheese wheel, characterized by a diameter of 22 cm, a height of 8 cm, and a mass of approximately 2.6 kg. Prior to testing, the wheel was verified as structurally flawless to establish the baseline acoustic response (healthy condition).

The artificially induced cavities were not intended to reproduce the exact morphology or surface characteristics of naturally occurring defects, such as fermentation pores or microcracks developed during cheese maturation. Instead, they were introduced as controlled and repeatable structural perturbations to provide a standardized proof-of-concept validation of the proposed actuation and acoustic monitoring methodology. Consequently, the present study does not aim to establish the minimum detectable size of natural defects, which will require dedicated investigations on real defective cheese wheels.

To empirically simulate the occurrence of internal defects, such as anomalous cavities typical of improper ripening, material was progressively extracted from the cheese matrix. The spatial references for the induced damage were defined relative to the front face, where the actuator strikes the cheese. The damage severity was qualitatively increased through five cumulative stages:

- Stage 1: A preliminary macroscopic void, consisting of an extracted volume of approximately 2 cm^3, was mechanically produced on the upper section of the cheese wheel.
- Stage 2: An equivalent structural cavity (2 cm^3) was introduced on the left lateral face of the specimen (Figure 11), progressively altering the structural integrity.
- Stage 3: A third identical volumetric extraction was performed centrally on the rear face, directly opposite the actuation point along the longitudinal axis.
- Stage 4: The spatial extent of the damage was increased by extending the longitudinal length of the rear central cavity by approximately 2 cm.
- Stage 5 (heavily damaged condition): A final, macroscopic cavity was excavated on the front face, in the center of the cheese wheel.



Figure 11. Detail of the progressive structural degradation (Stage 2). The image highlights the 2 cm^3 macroscopic cavity mechanically induced on the left lateral face of the aged Pecorino cheese wheel.

For each of these progressive stages, the automated system was operated to acquire a robust set of four validated Impulse Responses (IRs). This incremental approach was sufficient to induce measurable shifts in the modal response of the cheese matrix, allowing a qualitative assessment of the acoustic monitoring capabilities of the proposed setup.

The artificially induced cavities were not intended to reproduce the exact morphology or surface characteristics of naturally occurring defects, but rather to provide controlled and repeatable structural perturbations for the proof-of-concept validation of the proposed methodology. It should also be noted that the acoustic response depends not only on the severity of the structural degradation but also on the spatial location of the defect within the cheese matrix, since different defect positions perturb different vibration modes. Therefore, the present study was designed to demonstrate the sensitivity of the proposed methodology to progressive structural degradation rather than to isolate the individual effects of defect size, morphology, or location.

4. Experimental Results

This section presents and discusses the results obtained from the converter simulations, as well as the experimental data collected from the prototype implementation. In addition, it includes the analysis of the impact sound recordings acquired using microphones, providing a comprehensive evaluation of both the electrical performance and the acoustic behavior of the system under real operating conditions.

4.1. Power Converter Simulation and Experimental Results

The results of the simulation of the power converter are presented in Figure 12. As can be clearly observed, the reference current profile (red trace) is tracked accurately by the system response (blue trace). The actual current closely follows the desired reference value during the whole time interval. This demonstrates the effectiveness of the proposed closed-loop control strategy in achieving precise current regulation and confirms the good dynamic performance of the entire system.

The change in inductance follows the displacement of the plunger inside the solenoid. As the plunger moves toward the center of the energized coil, the magnetic reluctance decreases and the inductance increases, reaching its maximum value when the plunger is at the end of the pushing stroke. During the return motion, the opposite effect occurs, and the inductance progressively decreases back to its initial value. The obtained trend is consistent with the expected behavior of the magnetic circuit.

4.2. Acoustic Validation and Defect Detection Capability

While the previous section validated the electrical tracking performance of the power converter, this section focuses on the experimental validation of the proposed automated tapping system from an acoustic and diagnostic perspective. The evaluation of the interaction between the mechanical plunger and the cheese matrix is structured into two sequential phases. First, Section 4.2.1 analyzes the intra-class repeatability of the mechanical excitation to confirm the deterministic and reliable nature of the automated strike. Subsequently, based on this verified repeatability, Section 4.2.2 assesses the diagnostic sensitivity of the overall system by monitoring the evolution of the acoustic modal response as a function of the progressive structural degradation induced in the cheese specimen.

4.2.1. Acoustic Response and Test Repeatability

To validate the deterministic reliability of the closed-loop current-controlled actuator, the intra-class spectral variance of the acquired Impulse Responses (IRs) was evaluated. Figure 12 illustrates the comparison between the frequency response functions and their corresponding spectral residuals for four consecutive strikes, tested on both a healthy specimen (Figure 13a) and a heavily damaged one (Figure 13b).

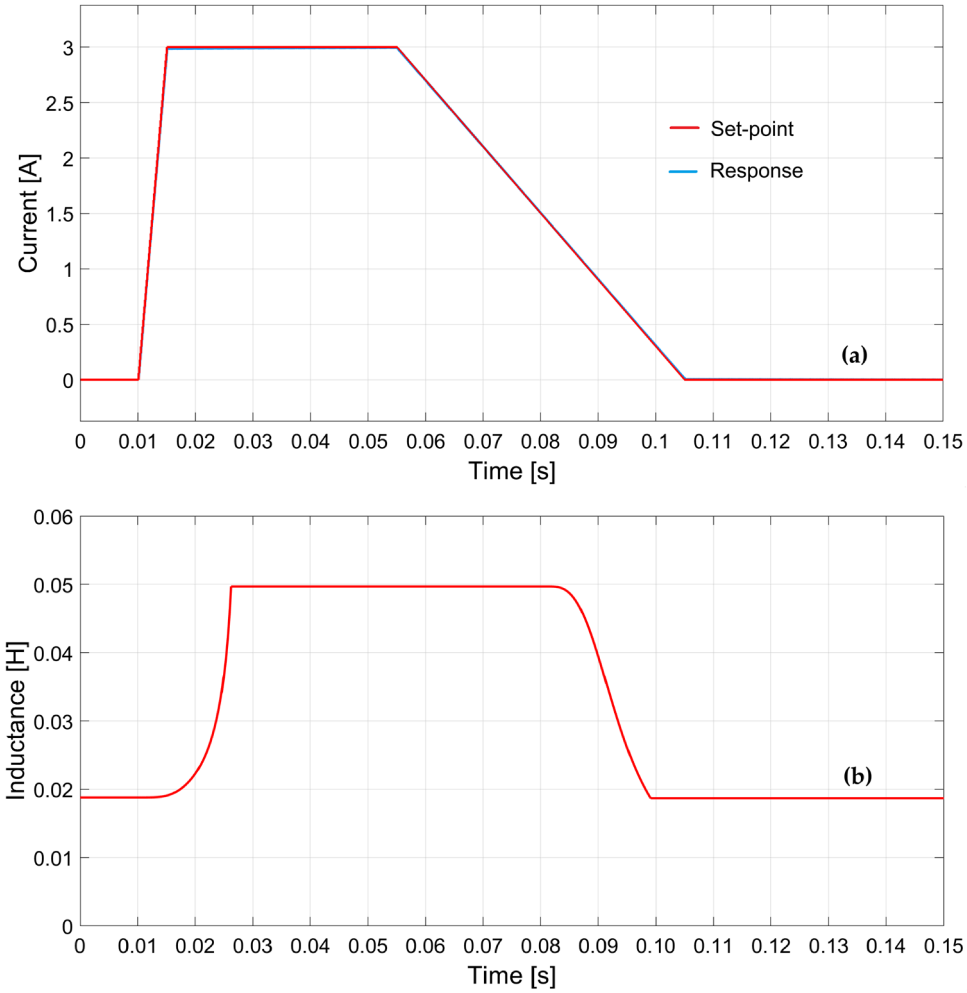


Figure 12. Set-point for driving the linear actuator and response current profiles (**a**). Inductance variation (**b**).

As visually evident, while physiological micro-deviations are expected due to the highly heterogeneous nature of the cheese crust, the overall modal envelope and the primary resonance peaks are strictly preserved across all repetitions. This confirms that the spectral morphology of the acoustic response is highly consistent for each structural condition. Furthermore, this consistency is maintained in both the healthy and heavily damaged scenarios, demonstrating that the deterministic nature of the mechatronic impact is independent of the target's structural integrity.

Quantitatively, the repeatability was confirmed by calculating the Mean Absolute Error (MAE) of the smoothed spectral residuals, as previously formalized in Section 3.3. The MAE evaluated for the healthy condition was strictly confined to 0.98 dB, while for the heavily damaged condition, it settled at an even lower 0.70 dB. These values, being tightly bounded below the 1 dB threshold, mathematically demonstrate that the intra-class variance is negligible. Consequently, this validates the robustness of the proposed mechatronic actuation system, proving that it delivers a highly repeatable mechanical excitation. More importantly, this minimal residual error is over an order of magnitude lower than the macroscopic spectral variations induced by internal structural defects, ensuring that the diagnostic information is not masked by instrumental uncertainty.

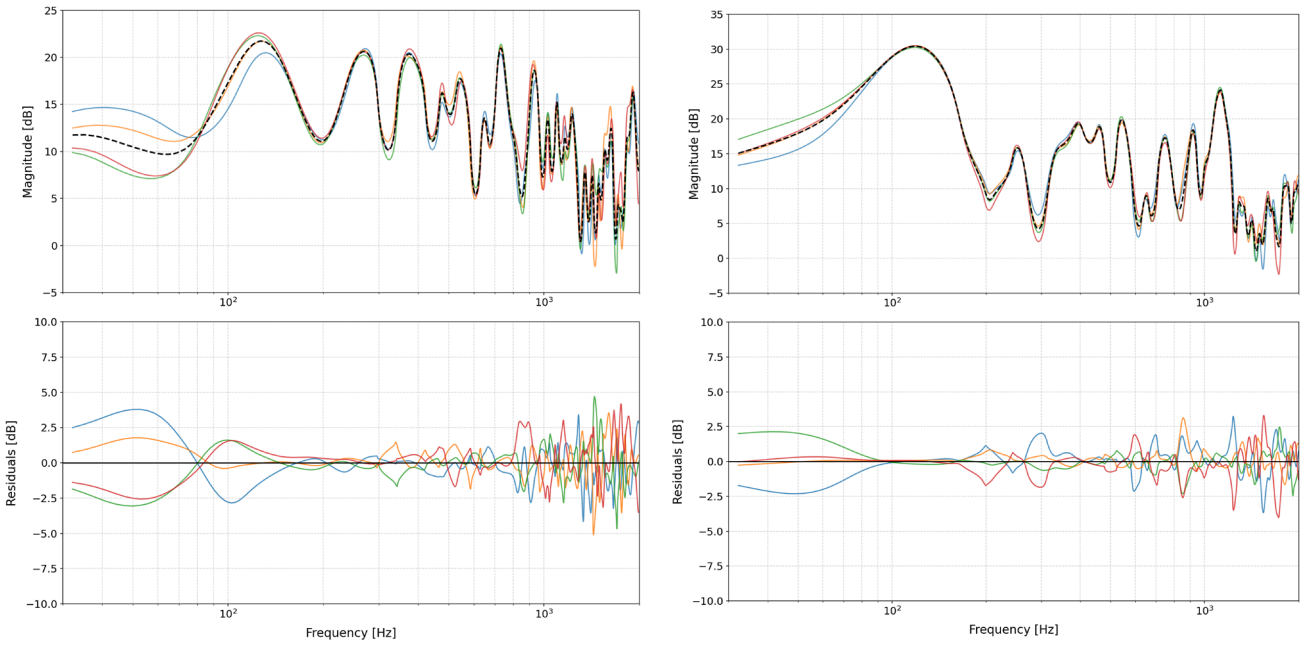


Figure 13. Comparison of the frequency response functions and spectral residuals across multiple impact repetitions (30–2000 Hz range): (**a**) healthy cheese specimen; (**b**) heavily damaged cheese specimen. The continuous curves represent different repetitions of the experiment, while the dashed line represents the ensemble average.

4.2.2. Sensitivity to Progressive Structural Degradation

Once the actuation repeatability was proven, the system's diagnostic sensitivity was assessed by analyzing the ensemble average spectra across the five progressive damage stages defined in the experimental protocol. Figure 14 presents the evolution of the acoustic modal envelope as the cheese matrix undergoes progressive volumetric extractions.

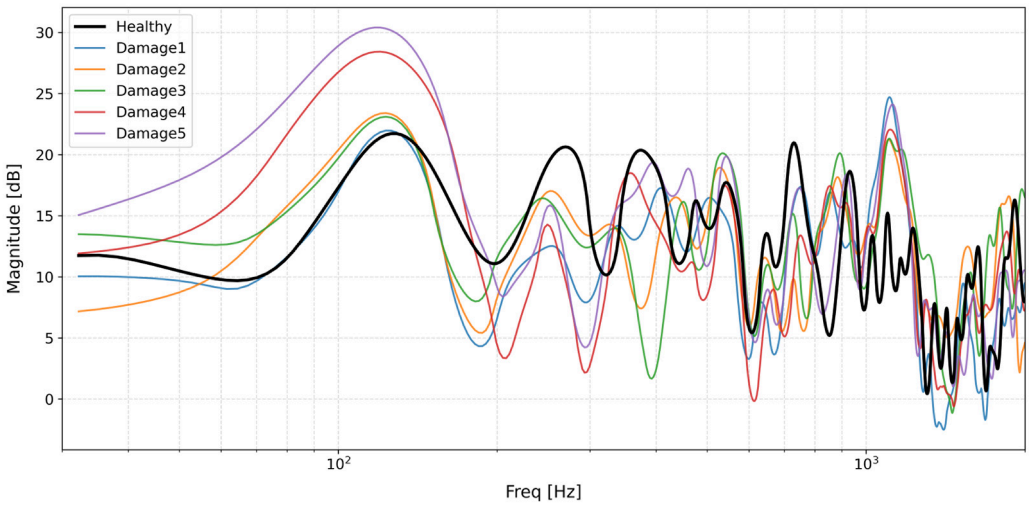


Figure 14. Mean spectrum comparison of the captured IRs as a function of damage severity within the 30–2000 Hz frequency domain. Each continuous curve represents the ensemble average of the experimental repetitions.

To quantitatively assess the diagnostic sensitivity of the mechatronic excitation, the spectral evolution of three key resonant modes was extracted and tracked across the progressive damage stages, as summarized in Table 5. The baseline curve (healthy condition)

exhibits a specific modal signature dictated by the mechanical impedance of the intact cheese wheel. As the structural degradation advances from Stage 1 to Stage 5, distinct elasto-acoustic phenomena emerge within the investigated bandwidth.

Table 5. Evolution of key spectral peaks (frequency and magnitude) as a function of the progressive structural damage.

Condition	Mode 1 (Shift and Increase)	Mode 2 (Shift and Attenuation)	Mode 3 (Damage Induced)
Healthy	128.91 Hz (21.72 dB)	269.53 Hz (20.64 dB)	Not detected
Damage 1	123.05 Hz (21.96 dB)	254.88 Hz (12.52 dB)	1107.42 Hz (24.71 dB)
Damage 2	123.05 Hz (23.40 dB)	251.95 Hz (17.03 dB)	1104.49 Hz (21.24 dB)
Damage 3	123.05 Hz (23.10 dB)	243.16 Hz (16.43 dB)	1107.42 Hz (21.31 dB)
Damage 4	120.12 Hz (28.43 dB)	249.02 Hz (14.28 dB)	1110.35 Hz (22.06 dB)
Damage 5	117.19 Hz (30.40 dB)	251.95 Hz (15.86 dB)	1122.07 Hz (24.12 dB)

Analyzing the lower portion of the spectrum, the primary resonance, initially located at 128 Hz in the healthy specimen, exhibits a progressive downward frequency shift and a concurrent increase in peak magnitude as the severity of the damage increases. From a mechanical perspective, while the volumetric extraction removes mass (which would theoretically increase the natural frequency), it introduces a severe discontinuity in the cheese matrix that drastically degrades the local stiffness. This reduction in structural stiffness dominates the dynamic response, resulting in the observed downward shift. Furthermore, the localized loss of dense material reduces the internal viscous damping, causing the resonance amplitude to increase.

The secondary resonance peak, prominently observed at 269 Hz in the healthy state, undergoes both a frequency shift and a severe magnitude attenuation. The introduction of internal mechanical discontinuities (voids) acts as a physical barrier to wave propagation, effectively disrupting the modal shape and dampening the acoustic energy at this specific wavelength. Finally, examining the higher frequency band, the continuous spectral monitoring reveals the sudden emergence of a peak at approximately 1107 Hz. This peak, completely absent in the healthy baseline, is immediately triggered by the introduction of the first macroscopic defect (Stage 1). It acts as a clear damage-induced marker, generated by the new boundary conditions and the localized resonances introduced by the artificial cavities.

Crucially, the spectral magnitude variations associated with these three phenomena are significantly larger than the instrumental uncertainty previously quantified in Section 4.2.1. While the intra-class spectral variance (MAE) of the mechatronic actuator was tightly bound below the 1 dB threshold, the damage-induced attenuations and amplifications exhibit dynamic variations of several decibels. This definitive margin confirms that the observed spectral shifts are genuine physical phenomena driven by the elasto-acoustic degradation of the cheese matrix, discarding the possibility of artifacts induced by measurement variability.

5. Conclusions

This work proposed and experimentally validated a current-controlled linear actuator system capable of generating optimized, repeatable mechanical excitation for automated acoustical inspection of hard cheeses. The proposed methodology integrates FEM-based actuator optimization, closed-loop current control, synchronized acoustic acquisition, and quantitative experimental validation.

This work presented the development and preliminary validation of an automated system for the acoustical inspection of hard cheeses based on a current-controlled linear electromagnetic actuator. The proposed solution was designed to reproduce the traditional

tapping procedure performed by expert cheese inspectors while providing a repeatable and objective excitation mechanism suitable for automated quality assessment.

FEM simulations were used to identify an optimal actuator current profile by including the dynamic behavior of the solenoid plunger system in the model. This resulted in a force profile that allows for a sharp, controlled impact of the plunger against the cheese, while also ensuring a smooth return motion to minimize unwanted mechanical vibrations that cause noise or acoustic disturbances. To precisely reproduce the desired excitation, a custom power converter with closed-loop current control was developed using MATLAB-Simulink simulations with PLECS Blockset. This demonstrated accurate tracking of the reference current profile, allowing for repeatable impact patterns.

A complete acoustic acquisition system based on a synchronized four-microphone array and an A2B-based data acquisition platform was also implemented. Experimental tests performed on an aged Pecorino cheese wheel demonstrated the excellent repeatability of the proposed mechatronic excitation system. The measured intra-class spectral variability remained below 1 dB for both healthy and damaged conditions, confirming that the generated impacts are highly consistent and suitable for reliable acoustic monitoring.

The proof-of-concept validation further showed that progressive structural degradations introduced into the cheese matrix produce clear and measurable modifications in the acoustic response. Significant shifts in resonance frequencies, variations in modal amplitudes, and the appearance of damage-induced spectral peaks were observed as the severity of the defects increased. These changes were substantially larger than the measurement uncertainty associated with the excitation system, confirming the capability of the proposed approach to detect structural anomalies.

Overall, the results demonstrate the feasibility of replacing subjective manual tapping with a controlled and repeatable automated system. Although the proposed actuator exhibited excellent repeatability under controlled experimental conditions, a direct quantitative comparison with traditional manual cheese beating performed by expert inspectors was beyond the scope of the present work. Such a comparison will be addressed in future studies to establish a practical baseline for impact repeatability and to evaluate the diagnostic performance of the automated system against current industrial practice.

Future work will focus on extending the experimental campaign to a larger number of cheese samples, maturation stages, and naturally occurring defects of different morphology and size in order to assess the detection limits of the proposed methodology, further improving the robustness of the current-controlled actuation system through thermal monitoring and compensation strategies, including coil temperature monitoring and online resistance estimation, as well as on the development of machine learning algorithms for automatic classification and defect detection based on the acquired acoustic signatures. The proposed methodology will also be validated under representative industrial operating conditions to assess its robustness against ambient acoustic noise and production-line disturbances.

Author Contributions: Conceptualization, A.T. and N.D.; methodology, A.T., N.D. and G.C.; software, A.T. and G.M.; validation, A.T. and G.C.; formal analysis, A.T. and G.C.; investigation, A.T. and N.D.; resources, N.D. and G.C.; data curation, A.T. and G.C.; writing—original draft preparation, A.T. and N.D.; writing—review and editing, A.T., N.D., C.C. and G.C.; visualization, A.T. and N.D.; supervision, A.T. and N.D.; project administration, A.T. and N.D. All authors have read and agreed to the published version of the manuscript.

Funding: This research received no external funding.

Institutional Review Board Statement: Not applicable.

Informed Consent Statement: Not applicable.

Data Availability Statement: The data presented in this study are available on request from the corresponding author due to privacy concerns.

Conflicts of Interest: The authors declare no conflicts of interest.

References

1. Cheese Market Size, Share & Trends | Industry Report. 2026–2033. Available online: https://www.grandviewresearch.com/industry-analysis/cheese-market-report (accessed on 8 June 2026).
2. Cheese Market Size, Share, Growth, Analysis Report. 2026–2034. Available online: https://www.fortunebusinessinsights.com/cheese-market-104293 (accessed on 8 June 2026).
3. La Filiera Lattiero Casearia Italiana Cresce e si Rafforza sui Mercati Esteri—Ismea. Available online: https://www.ismea.it/flex/cm/pages/ServeBLOB.php/L/IT/IDPagina/13401 (accessed on 8 June 2026).
4. Specifications and Legislation. Available online: https://www.parmigianoreggiano.com/consortium-specifications-and-legislation (accessed on 8 June 2026).
5. Performance Record nel 2024 per Parmigiano e Grana. Available online: https://informatorezootecnico.edagricole.it/featured/performance-record-nel-2024-per-parmigiano-e-grana/ (accessed on 8 June 2026).
6. Ahranjani, P.J.; Ahranjani, P.J.; Dehghan, K.; Esfandiari, Z.; Ferrentino, G. Advances in spectroscopic techniques for the detection of cheese adulteration: A systematic review. *Food Chem. X* **2025**, *29*, 102685. [CrossRef] [PubMed]
7. Lei, T.; Sun, D.-W. Developments of nondestructive techniques for evaluating quality attributes of cheeses: A review. *Trends Food Sci. Technol.* **2019**, *88*, 527–542. [CrossRef]
8. McQueen, D.H.; Wilson, R.; Kinnunen, A.; Jensen, E.P. Comparison of two infrared spectroscopic methods for cheese analysis. *Talanta* **1995**, *42*, 2007–2015. [CrossRef] [PubMed]
9. Lerma-García, M.J.; Gori, A.; Cerretani, L.; Simó-Alfonso, E.F.; Caboni, M.F. Classification of Pecorino cheeses produced in Italy according to their ripening time and manufacturing technique using Fourier transform infrared spectroscopy. *J. Dairy Sci.* **2010**, *93*, 4490–4496. [CrossRef] [PubMed]
10. Cevoli, C.; Cerretani, L.; Gori, A.; Caboni, M.F.; Gallina Toschi, T.; Fabbri, A. Classification of Pecorino cheeses using electronic nose combined with artificial neural network and comparison with GC–MS analysis of volatile compounds. *Food Chem.* **2011**, *129*, 1315–1319. [CrossRef] [PubMed]
11. de Angelis Curtis, S.; Curini, R.; Delfini, M.; Brosio, E.; D'Ascenzo, F.; Bocca, B. Amino acid profile in the ripening of Grana Padano cheese: A NMR study. *Food Chem.* **2000**, *71*, 495–502. [CrossRef]
12. Maestrello, V.; Solovyev, P.; Stroppa, A.; Bontempo, L.; Franceschi, P. 1H NMR profiling and chemometric analysis for ripening and production characterization of Grana Padano cheese. *Food Chem.* **2024**, *456*, 139986. [CrossRef] [PubMed]
13. Chuquizuta, T.; Cieza, Y.; González, J.; Juarez, M.; Castro-Giraldez, M.; Fito, P.J.; Castro, W. Emerging Spectrophotonic Technologies to Predict the Maturation Time of Swiss-Type Cheese: Dielectric Spectroscopy vs. Portable NIR. *Processes* **2026**, *14*, 1022. [CrossRef]
14. Mendez, J.M.C.; Susanibar, L.K.M.; Laura, D.J.M.; Jimenez, C.S.M. Cheese Production Based on Industry 4.0 Automation and Simulation in the Company 'Vakilact'. In *Proceedings of the 2024 7th International Conference on Robotics, Control and Automation Engineering (RCAE)*; IEEE: Wuhu, China, 2024; pp. 451–459. [CrossRef]
15. König, N.; Nienhaus, M.; Grasso, E. Analysis of Current Ripples in Electromagnetic Actuators with Application to Inductance Estimation Techniques for Sensorless Monitoring. *Actuators* **2020**, *9*, 17. [CrossRef]
16. Wang, S.; Weng, Z.; Jin, B. A Performance Improvement Strategy for Solenoid Electromagnetic Actuator in Servo Proportional Valve. *Appl. Sci.* **2020**, *10*, 4352. [CrossRef]
17. Lu, M.; Yuan, Z.; Yi, X. Magnetic Field Analysis and Thrust Verification of Solenoid Actuator Based on Subdomain Method. *Machines* **2024**, *12*, 354. [CrossRef]
18. Plavec, E.; Petrinić, M.; Vidović, M. Improving the Force and Time Response of a DC Solenoid Electromagnetic Actuator by Changing the Lower Core Angle. *J. Electromagn. Eng. Sci.* **2021**, *21*, 95–103. [CrossRef]
19. Wang, S.J.; Weng, Z.D.; Jin, B.; Cai, H.X. Multi-objective genetic algorithm optimization of linear proportional solenoid actuator. *J. Braz. Soc. Mech. Sci. Eng.* **2021**, *43*, 60. [CrossRef]
20. Lu, S.; Wang, C.; Luo, A.; Li, Y.; Gao, G.; Gao, J.; Cheng, Z.; Liu, X. Dynamic and steady-state performance analysis of a linear solenoid parallel elastic actuator with nonlinear stiffness. *Nonlinear Dyn.* **2023**, *111*, 21507–21534. [CrossRef]
21. Abedinifar, M.; Ertugrul, S.; Tayyar, G.T. Design optimization of a solenoid actuator using particle swarm optimization algorithm with multiple objectives. *Adv. Mech. Eng.* **2022**, *14*, 168781322211357. [CrossRef]
22. Shang, R.; Liu, P.; Quan, W.; Ouyang, Y. Comparative Analysis of Armature Structure on Constant Force Characteristics in Long-Stroke Moving-Iron Proportional Solenoid Actuator. *Actuators* **2024**, *13*, 408. [CrossRef]

23. Fan, X.; Yin, J.; Lu, Q. Design and Analysis of a Novel Composited Electromagnetic Linear Actuator. *Actuators* **2021**, *11*, 6. [CrossRef]
24. COMSOL 6.4—Computing Electromagnetic Forces and Torques. Available online: https://doc.comsol.com/6.4/doc/com.comsol.help.acdc/acdc_ug_modeling.06.20.html (accessed on 15 June 2026).
25. Gomis-Bellmunt, O.; Campanile, L.F. *Design Rules for Actuators in Active Mechanical Systems*; Springer: London, UK, 2010. [CrossRef]
26. A^2B Automotive Audio Bus Technology. Available online: https://www.analog.com/en/solutions/a2b-automotive-audio-bus.html (accessed on 8 June 2026).
27. Toscani, A.; Rocchi, N.; Pinardi, D.; Binelli, M.; Saccenti, L.; Farina, A.; Pavoni, S.; Vanali, M. Low-cost Structural Health Monitoring System for Smart Buildings. In *2022 Second International Conference on Sustainable Mobility Applications, Renewables and Technology (SMART)*; IEEE: Cassino, Italy, 2022; pp. 1–7. [CrossRef]
28. Toscani, A.; Rocchi, N.; Pinardi, D.; Binelli, M.; Saccenti, L.; Farina, A.; Pavoni, S.; Vanali, M. Low-Cost Condition Monitoring System for Smart Buildings and Industrial Applications. *IEEE Trans. Ind. Appl.* **2024**, *60*, 1870–1878. [CrossRef]
29. Toscani, A.; Immovilli, F.; Pinardi, D.; Cattani, L. A Novel Scalable Digital Data Acquisition System for Industrial Condition Monitoring. *IEEE Trans. Ind. Electron.* **2024**, *71*, 7975–7985. [CrossRef]
30. Pinardi, D.; Toscani, A.; Binelli, M.; Saccenti, L.; Farina, A.; Cattani, L. Full-Digital Microphone Meta-Arrays for Consumer Electronics. *IEEE Trans. Consum. Electron.* **2023**, *69*, 640–648. [CrossRef]
31. Rocchi, N.; Toscani, A.; Pinardi, D.; Binelli, M.; Chiesi, L.; Farina, A.; Bonomi, E.; Tronchin, L. A Modular, Low Latency, A 2 B-based Architecture for Distributed Multichannel Full-Digital Audio Systems. In *2021 Immersive and 3D Audio: From Architecture to Automotive (I3DA)*; IEEE: Bologna, Italy, 2021; pp. 1–8. [CrossRef]
32. Rocchi, N.; Toscani, A.; Chiorboli, G.; Pinardi, D.; Binelli, M.; Farina, A. Transducer Arrays Over A2B Networks in Industrial and Automotive Applications: Clock Propagation Measurements. *IEEE Access* **2021**, *9*, 118232–118241. [CrossRef]

Disclaimer/Publisher's Note: The statements, opinions and data contained in all publications are solely those of the individual author(s) and contributor(s) and not of MDPI and/or the editor(s). MDPI and/or the editor(s) disclaim responsibility for any injury to people or property resulting from any ideas, methods, instructions or products referred to in the content.